Electron Cryotomography of Bacterial Secretion Systems

Capstone Project Report for

Physics 492R

by

Edward Krzymowski

Submitted to the Department of Physics in partial fulfillment

of graduation requirements for the degree of

Bachelor of Science – Applied Physics.

Brigham Young University

December 2022

Abstract

Electron Cryotomography (Cryo-ET) is an important imaging technique used by scientists. It uses cryogenic sample preparation, an electron microscope, and powerful image processing software to create high-resolution 3D views of cells and the structures within them. Cryo-ET has been a valuable tool for discovering many novel features about the functions of a wide variety of bacterial species. I was closely involved in two Cryo-ET research projects during my time at BYU. This paper will discuss both projects, as well as the principles of Cryo-ET and potential future applications of such research.

Acknowledgements

I would like to give special thanks to Brigham Young University, the Department of Physics and Astronomy, the Jensen Lab, and Dr. Grant Jensen for their generous support of this research. I am also very appreciative of my project leads, Drs. Georges Chreifi and Mohammed Kaplan, for their training and assistance.

Contents

List of Figures

1. Introduction

1.1 Fundamentals of Cryo-ET

Cryo-ET is an imaging technique used by scientists to create high resolution images of samples. It is done using a combination of three important technologies: cryogenics, electron microscopy, and tomography. The "cryo" prefix refers to the use of a cryogenic liquid to freeze the samples before the microscopy is performed (1). Electron microscopy uses a transmission electron microscope to produce high resolution images of the specimen (1). Finally, tomography is a generic method of imaging in which the 3D structure of an object can be created by combining 2D projections. It is commonly used in medicine in the technique computerized axial tomography (CAT) scan (1).

Cryo-ET was developed in the 1980s to address some of the challenges of attempting to view biological material using a standard electron microscope. Although transmission electron microscopes are powerful enough to resolve sample details on nearly an atomic scale, qualities inherent to their operation prevent them from being used effectively for things such as cells. For example, the central column in an electron microscope must be maintained at a high vacuum in order to function. If a cell sample were to be inserted into the column under these conditions, the water in the individual cells would instantly boil away causing the cells to be destroyed (2). For many years, scientists attempted to solve these problems with methods such as using chemicals to fix and dehydrate cells, and/or by embedding the cells in resin. These methods were an improvement over previous attempts but caused artifacts and the loss of many details (2).

Eventually it was determined that the cell samples could simply be frozen using cryogenic liquid. Slower freezing procedures could not be used because water expands during a slow freezing process, which would destroy the cellular structure. Using a cryogenic liquid, such as ethane, removes the kinetic energy from the water molecules before they can bond with adjacent molecules. This type of ice is an amorphous solid and is referred to as "vitreous" ice (2). This method of freezing preserves the integrity of the structures within the cell, thus allowing them to be viewed with the electron microscope. Once the samples have been frozen, they are loaded into the electron microscope and imaged. Images of the sample are taken from several different angles. The images are then back projected and combined to form a 3D reconstruction of the sample called a tomogram (1) (Fig. 1).

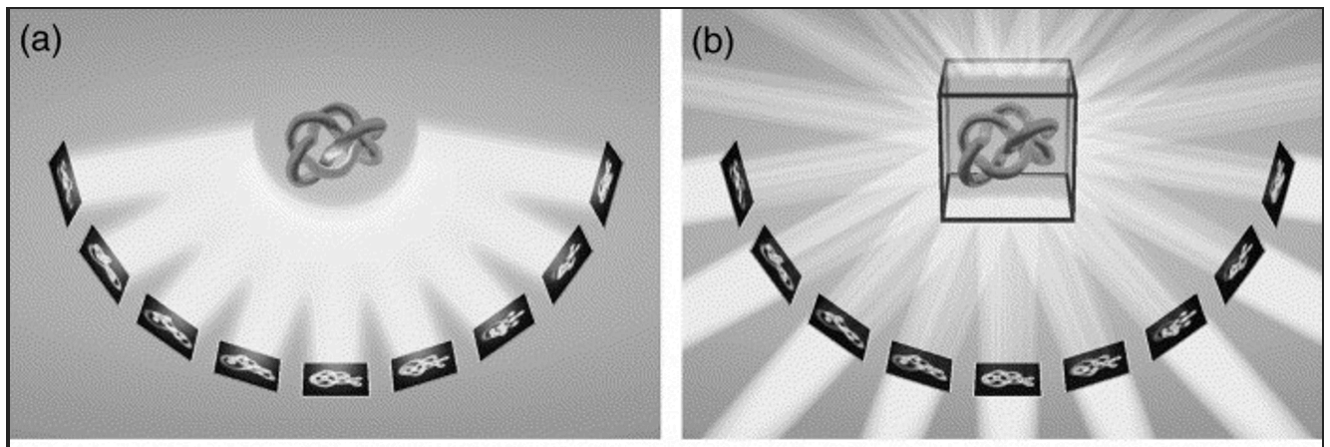
Fig. 1 An illustration of tomography.

(A) Projections of the sample are first taken from several different angles. (B) Those images are then back-projected and combined to get a 3D reconstruction of the original (figure reproduced from (3)).

One of the most valuable techniques available with cryo-ET is sub-tomogram averaging. This technique allows researchers to overcome one of the significant weaknesses of cryo-ET, image quality. Typically, the quality of cryo-ET images is quite poor, due to both intrinsic statistical noise (caused by a small number of electrons per pixel of the image detector), and Landau noise (caused by a large distribution of signal levels of the individual electrons detected by the image detector). In sub-tomogram averaging, the researcher will manually select a large number of the desired structures in the tomograms (a process known as "particle picking"), and then use image processing software (such as IMOD or EMAN2) to average all of the images together. This decreases much of the noise and allows for greater resolution (34) (Fig 2). In the end cryo-ET, combined with sub-tomogram averaging, enables the acquisition of 3D images of cellular samples in a relatively unmarred state to a high resolution of ~4nm, sufficient to see large macromolecular nanomachines (2).
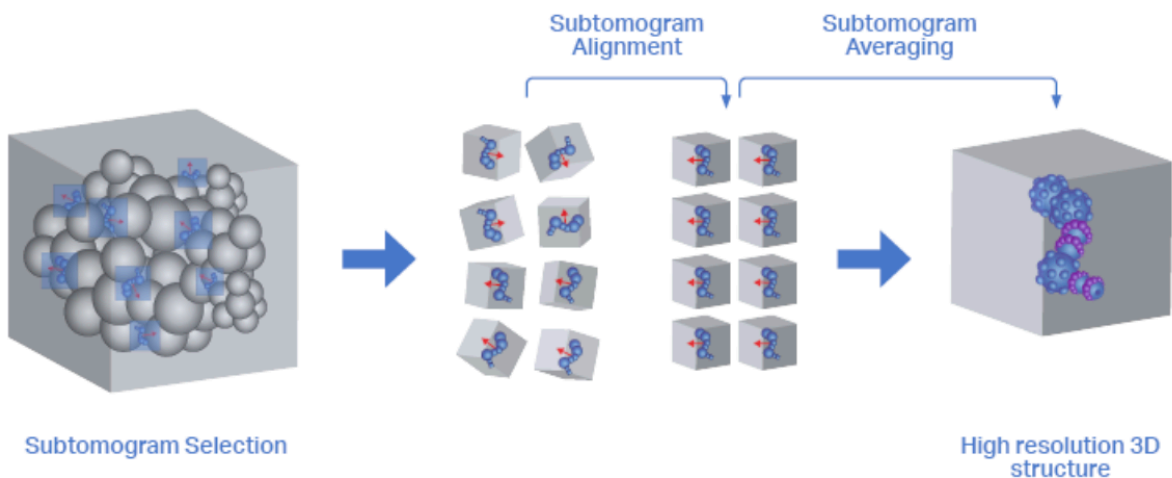

Fig. 2 An illustration of sub-tomogram averaging

A large number of particles (highlighted in blue) are picked from the tomogram. Image

processing software is used to align and average the particles. This increases the signal-

to-noise ratio and creates a high-resolution 3D image (figure reproduced from (39)).

1.2 Applications of Cryo-ET

Since its implementation into the field of microbiology, cryo-ET has been used with

great success to image many intracellular structures of various types, especially in bacteria. Due

to its ability to obtain high resolution of biological structures, Cryo-ET has been an extremely

powerful tool for detailed analysis of these structures. This has shown that bacterial cells are far

more complex and organized than was previously believed.

Before Cryo-ET was available, prokaryotic cells were thought to largely lack cytoskeletal

structures. The direct visualization of these cells has allowed the discovery of a large variety of

cytoskeletal components in bacteria. Researchers have been able to find many examples of

these, such as the discovery of MamK (which is an actin homologue that assists in aligning

microcompartments in magnetotactic bacteria) (4) or FtsZ (another protein which controls cell

division in almost all bacterial species) (5). This technology has also proved instrumental in

showing many structures within bacterial cells which were once thought to be unstructured,

but which are in reality highly organized. This includes complexes such as chemosensory arrays

(6) and microcompartments for storing nutrients and optimizing metabolism (7,8).

More recently, significant effort has been expended to attempt to learn more about

bacterial secretion systems. These protein complexes are used by bacteria to perform a wide

variety of tasks, ranging from DNA transfer to attacking other cells, and harnessing them could

lead to beneficial technological advances for humanity. For example, a greater understanding of bacterial secretion systems could enable the development of much safer and more effective antibiotic drugs. There are many bacterial species that are resistant to classical antibiotics but could still be successfully nullified by drugs designed to target their secretion systems. In addition, due to the specificity of these systems, such drugs could also allow for successful elimination of the pathogenic bacteria without decimating the naturally beneficial human bacterial biome (28).

Power generation is another promising area of bacterial research. As concerns about energy availability increase around the world, largely due to cost and environmental concerns, more researchers are looking for alternative sources. Some have found that, using a combination of natural bacterial capabilities and gene editing, bacteria can be used to produce various forms of energy. One example is *Streptomyces coelicolor*, which uses a Type VII Secretion System and can be altered to produce polycyclopropanated fatty acids (POP-FAs). These can then be used in place of traditional fossil fuels, with the advantages of being significantly more renewable and having superior thermal properties to hydrocarbon fuels (29,30). Other researchers have been working on creating microbial fuel cells (MFCs) which use bacteria such as *Geobacter* or *Shewanella* to generate an electrical current. This method of power generation has an added benefit in that these bacteria could feed off organic compounds commonly found in wastewater (31). Similar bacterial technologies show promise in areas such as cancer treatment (32) and nanotechnology (33). These types of biotechnology have the potential to dramatically improve the world we live in. However, they require an intimate knowledge of bacteria, their internal structures, and their functions.

2. The *Porphyromonas gingivalis* Type IX Secretion System

2.1 Intro to the T9SS

Porphorymonas gingivalis is a Gram-negative anerobic bacteria. It is pathogenic to humans and causes periodontitis, an inflammatory disease that can damage or destroy teeth. It has also been implicated in the development of certain types of rheumatoid arthritis. While *P. gingivalis* is naturally found in the human oral biome, it can become highly destructive when allowed to proliferate (23).

P. gingivalis utilizes a strategy of invading host cells and replicating and spreading within them to help it evade detection by the body's immune system. These bacteria secrete a variety of virulence factors, including capsular polysaccharide and gingipains, in order to successfully carry out this invasion (24). One of the primary tools of secretion for *P. gingivalis* is the Type IX Secretion System (T9SS), which secretes ~30 different effector proteins. Among these is peptidylarginine deiminase (PPAD), which is responsible for the host protein citrullination that has been linked to rheumatoid arthritis (21).

Although many of the structural components of the T9SS are already known, the overall organization of these components has not yet been fully elucidated. Among the sub-complexes which are known are the PorK/PorN complex which forms a large ring-like structure and is localized to the outer membrane, and the PorM/PorL ring which is localized to the inner membrane and extends into the periplasm (22). In addition, there is a known complex comprised of PorU/PorV/PorQ/PorZ which anchors the T9SS substrates to the surface of the

cell (26). The purpose of this project was to gain a greater understanding of the structure and function of the T9SS by using cryo-ET to visualize it *in situ*.

2.2 Preparation of Bacterial Culture for Cryo-ET

Bacterial cell samples were prepared as described in (36) with the following particulars: P. gingivalis strain W50ABK*WbaP mutant cells were streaked onto blood agar plates containing trypticase soy agar and 5% defibrinated horse blood. Plates were incubated anaerobically at 37 °C for 3-4 days until colonies appeared. A single colony was then used to inoculate 5 mL of brain-heart infusion broth enriched with tryptic soy (TSBHI) (25 g/L Tryptic soy, 30 g/L BHI) and supplemented with 0.5 mg/mL cysteine, 5 g/mL hemin and 5 g/mL menadione. Cell cultures were grown anaerobically at 37°C until they reached OD_{600} of 1.0, indicating early stationary phase. Cells were then harvested by centrifugation at 10000 g for 10 minutes and resuspended in 20 mM Tris-HCl, pH 7.5 buffer containing 20 mM NaCl and 10 mM MgCl 2 and 10 nm colloidal gold beads (Ted Pella, Inc., Redding, CA, USA) pre-treated with 5% (w/v) bovine serum albumin. Copper R2/2 200 Quantifoil holey carbon grids (Quantifoil Micro Tools GmbH, Jena, Germany) were glow discharged before adding 3-4 µL of the cell mixture. EM grids were subsequently blotted and plunge frozen in a liquid ethane/propane mixture using an FEI Vitrobot Mark IV (Thermo Fisher Scientific) and stored in liquid nitrogen until data acquisition (36).

2.3 Cryo-ET Data Acquisition, Processing, and Sub-tomogram Averaging.

Cryo-ET data were acquired as described in (36), with the following particulars: Cryo-ET data were acquired on a Titan Krios G3i (Thermo Fisher Scientific) equipped with a Gatan

energy filter and a K3 electron detector (Gatan)operating in electron counting mode with correlated-double sampling. The *P. gingivalis* ABK⁻ tilt series were obtained using the SerialEM software package, with a tilt range of -60° to +60°, tilt increments of 3° per tilt, a total dose of ~150 e-/ $Å^2$, and target focus ranging from 5-8 μm under focus. Images were aligned, contrast transfer function corrected, and the three-dimensional reconstructions of the tilt-series were done using the EMAN2 software package (Chen et al., 2019). A total of 1960 tilt series were collected with 923 particles being manually identified and selected from the tomogram reconstructions. The particles were then extracted using a box size of 80 (with x2 binning), and aligned using EMAN2 3D refinement software, with c2 symmetry imposed (36).

2.4 Results

I was tasked with picking particles from this *P. gingivalis* dataset. An example of one of these particles in shown in figure 3. The particles were then averaged by Georges Chreifi to obtain the sub-tomogram average shown in figure 4. Some of the identifying features of the T9SS can be observed, most notably the PorK/N ring. Additional densities, possibly including the PorM/L complex can also be seen beneath the PorK/N ring (22). The proposed structure in figure 5 is provided as a reference. This sub-tomogram average helps to further verify parts of the already proposed structure for the T9SS. However, additional investigation is required to confirm the identity of the other densities that were observed. This project is ongoing and so it is likely that more information will be gleaned from these sub-tomogram averages in the future.
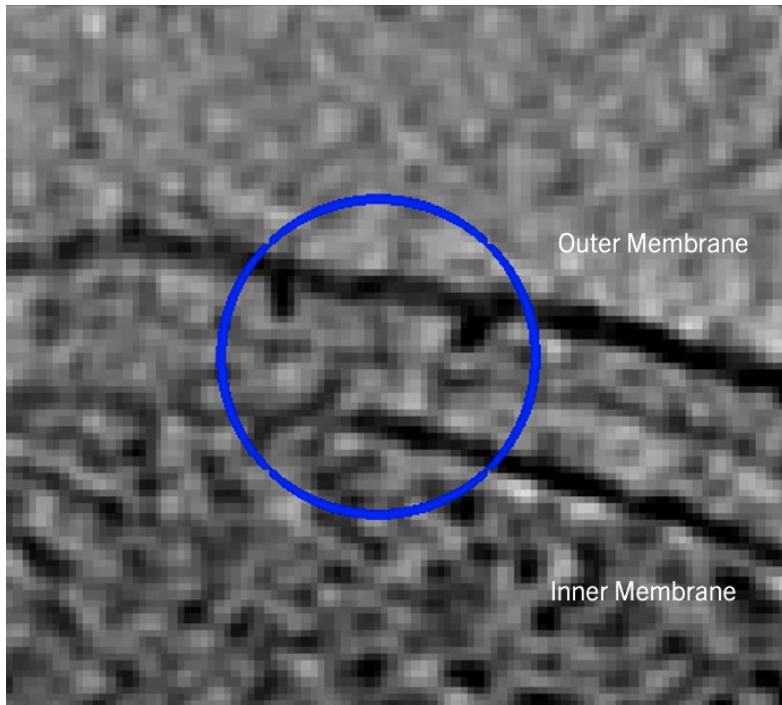
Fig. 3 T9SS Particle

Example of a T9SS particle taken from a single tomogram. Inner/outer membranes are labeled.

The side profile of a PorK/N ring can be seen. Other densities in the periplasmic region and

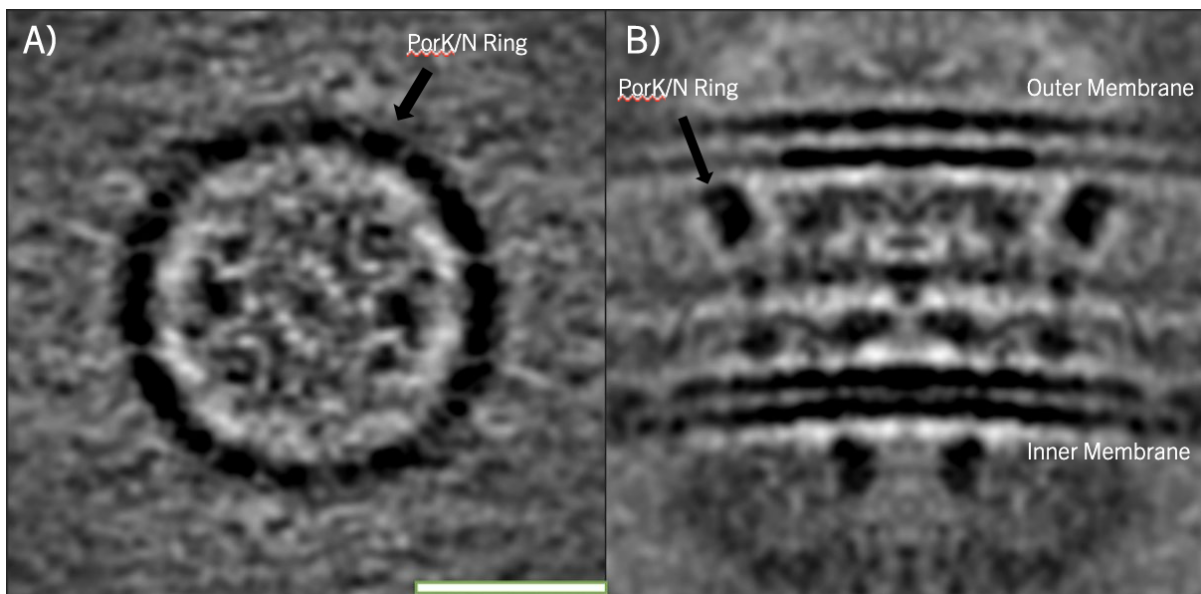penetrating through the IM can be seen.

Fig. 4 Sub-tomogram averages of T9SS

(A) Top view of T9SS complex. PorK/N ring is clearly identifiable. (B) Side view of T9SS complex. Inner/outer membranes are labeled. PorK/N ring is again observable, along with other densities, including what could be PorM/L complex near the inner membrane. Scale bar is ~50nm.
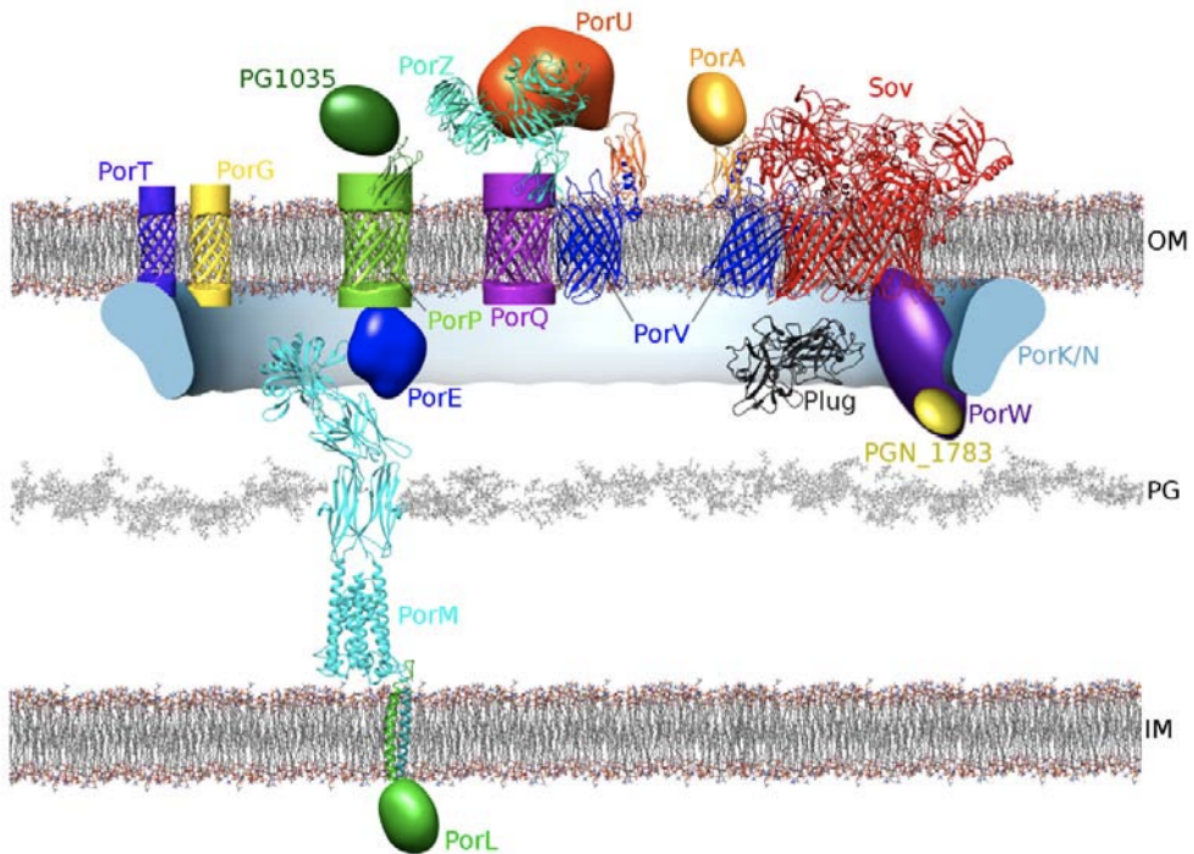

Fig. 5 Proposed Organization of the T9SS components within the PorK/N rings

Proposed structural organization of T9SS in *P. gingivalis.* Components of this complex are not discussed in this work, it is only for comparison to the sub-tomogram average shown above (figure reproduced from (36)).

3. The *Coxiella burnetii* Type IV Secretion System

3.1 Intro to T4SS

Coxiella burnetii is a species of Gram-negative pathogenic bacteria. It is responsible for the disease known as Q Fever. This disease commonly leads to flu-like symptoms, but in more severe cases can cause things such as hepatitis, myocarditis, and pneumonia (9). This bacterial species has a biphasic developmental cycle which consists of active and dormant stages. These stages are known as the small cell variant (SCV) and the large cell variant (LCV) (14).

External to the body, *C. burnetii* remains in the highly stable SCV state. It is in this state that the bacteria are commonly spread through the inhalation of contaminated aerosols. Once inside the host the SCVs target alveolar macrophages (13). They then enter the metabolically active LCV phase. This process of maturation from inactive to active state is mediated in large part by the *C. burnetii* Dot/Icm (defective in organelle trafficking/intracellular multiplication) Type IV Secretion System (T4SS).

The *C. burnetii* secretion system belongs to a subset of these complexes known as T4BSS. The *C. burnetii* T4BSS protein complex secretes more than 130 different effector proteins into the host cell (35). This affects the internal functions of the host cell in ways which are vital for the intracellular replication of *C. burnetii*. Thus, the *C. burnetii* T4BSS plays a vital role in the pathogenicity of this bacterial species.

In order to gain a greater understanding of the structure and function of the *C. burnetii* T4BSS, this research project was focused on imaging this protein complex using cryo-ET.

Throughout this project I was working contemporaneously with another research team using the same data. This section will discuss my work, as well as the results they compiled.

3.1 Preparation of Bacterial Culture for Cryo-ET

The bacterial cell cultures were prepared as described in (37) with the following particulars: The *Coxiella burnetii* strain which was used was the Nine Mile phase II (clone 4, RSA 439) strain. For the samples which were purified from eukaryotic host cells, *C. burnetti* was grown in African green monkey kidney (Vero) fibroblasts (CCL-81; American Type Culture Collection). These are cultured in RPMI medium (Invitrogen, Carlsbad, California) and supplemented with 2% fetal bovine serum as described in reference (15). Vero host cells were briefly infected in 150-cm^2 flasks for 4 weeks without changing the growth medium. The cells were incubated at 37 C in 5% CO2 during the first week. Afterwards, the flasks containing the cell samples were kept at room temperature with their caps tightened for three weeks. The bacterial cells were next purified from the infected eukaryotic cells using Renografin density gradient centrifugation (16). Purified SCV cells were resuspended in K-36 buffer (0.1 M KCl, 0.015 M NaCl, 0.05 M potassium phosphate, pH 7.0) and stored at -80 C until they were thawed before plunge-freezing as described below (37).

Alternatively, *C. burnetii* (wilt type Nine Mile phase II strain or an isogenic dot/icm mutant of this strain) was grown under axenic cultivation conditions as described in (17,18). To cultivate *C. burnetii*, ACCM-2, which is a modified ACCm medium, was used (64). In the ACCM-2 medium, 1 mg/ml methyl-β-cyclodextrin (Mβ-CD) is used to replace 1% FBS. Bacterial cells were

then cultured in this medium using T-75 flasks or 0.2-µm-pore-size-filter-capped 125-ml

Erlenmeyer flasks with 20 ml of medium, T-25 flasks with 5 ml of medium, or 3 ml of medium in

each well of a 6-well tissue culture plate. Bacterial cultures were kept in a CO-170 incubator

(New Brunswick Scientific, NJ) with the following conditions: 37 C in a 2.5% O2 and 5% CO2.

Cells were then washed and resuspended in either PBS pH 7.2 or Citrate buffered saline pH 4.75

(PBS + 10 mM citrate). They were then frozen at -80 C until they were thawed prior to plunge-

freezing (37).

The *C. burnetii* cell samples were grown in host cell-free second-generation acidified

citrate cysteine media (ACCM-2). Cell samples were used which had been grown in the ACCM-2

medium for 5 and 14 days. This allowed for a variety of cells in both the SCV and LCV stages.

Both samples were imaged using a cryo-electron microscope at CalTech, resulting in a series of

tilt-series. That data was sent to me through the Jensen Lab tomography database (14). The tilt

series were compiled into tomograms through EMAN2 image processing software (11). The

T4BSS were visually identified and selected and a box size of 96 (with x2 binning) was used. The

particles were extracted and averaged using the same EMAN2 software (37).

3.3 Cryo-ET Sample Preparation and Imaging

The bacterial samples were prepared for Cryo-ET as described in (37) with the following

particulars: R2/2 carbon-coated 200 mesh copper Quantifoil grids (Quantifoil Micro Tools) were

first glow-discharged for 60 seconds. 4 µL of cells were thawed from a -80°C stock and then 1 µL

of BSA-treated 10-nm gold solution was added. The cells/gold combination was pipetted onto

the grids using a Vitrobot chamber (FEI) at 100% humidity. The extra fluid was blotted off of the

samples using Whatman filter paper. The grids were then plunge-frozen in a liquid

ethane/propane mixture. The samples were imaged using an FEI Polara 300 keV field emission

gun electron microscope (FEI, Hillsboro, OR, USA) which was equipped with a Gatan image filter

and K2 Summit direct electron detector in electron counting mode (Gatan, Pleasanton, CA,

USA). Data were collected using the UCSF Tomography software (19) with each tilt series

ranging from −60° to 60° in 1°, 2° or 3° increments, an underfocus of ~7 μm, an electron dose of

130 e- /Å2 , and a pixel size of 3.9 Å (37).

3.4 Image Processing and Sub-tomogram Averaging

The three-dimensional reconstructions of the tilt-series were done using the EMAN2

software package (Chen et al., 2019). T4BSS particles were manually identified and selected

from the tomograms in each dataset. The particles were then extracted using a box size of 96

from the tomograms with x2 binning (8.06 Å/pix). The EMAN2 program e2spt_sgd_new.py was

used to generate an initial model of the T4BSS. A cylindrical mask was used to improve the

clarity of the sub tomogram average (37).

The researchers working contemporaneously with me used a total of 88 tomograms of

C. burnetii grown at pH 7 and 69 tomograms of *C. burnetii* grown at pH 4. From those they

managed to acquire 726 T4BSS particles from those cells grown at pH 7, and 414 T4BSS

particles from those grown at pH 4. Those particles were also extracted at a box size of 96, with

x2 binning (8.06 Å/pix). EMAN2 was used to generate initial model using a subset of 60 high-

quality particles at 4x binning. Initial models with C1 symmetry were generated using the

default parameters in the e2spt_sgd_new.py program. Those C1 models were then aligned to a

symmetry axis and used as references for initial models with C13 symmetry. All initial models were filtered to 50 Å resolution and used for subsequent sub-tomogram refinement. The extracted particles from both datasets were used for the sub-tomogram averaging with either C1 or C13 symmetry. Those particles were subjected to two rounds of 3D particle orientation refinement, 2D sub-tilt translation refinement, and sub-tilt translation & rotation refinement, followed by a sub-tilt defocus refinement. In a final step, soft masks for either the Outer Membrane Core Complex (OMCC) or the Inner Membrane (IM) were applied to focus the alignment of the particles to each respective region (37).

3.5 Results

For this project I was tasked with picking the particles from the *C. burnetii* T4SS dataset, and then attempting to get a sub-tomogram average of them. I picked 288 particles from 562 tomograms. In many of the tomograms there were extracellular densities that appeared to have been secreted by the T4SS. We were interested in looking at both T4SS particles in a resting and in a secreting state, so both types were selected and differentiated. Examples of both are shown in figure 5. The lab which was working contemporaneously managed to compile their results before I was able to get a good sub-tomogram average, at which point I stopped work on this project, and their results are discussed below.

In the work done by the other lab, 512 T4SS particles were averaged. This resulted in a sub-tomogram average with a resolution of 2.5-4.5 nm (37). This average was done using cells that had been grown in the ACCM-2 medium for five days and then resuspended in phosphate buffer saline pH 7.2. Initially, the densities associated with the outer membrane (OM) and the

periplasmic region were resolved nicely, however the densities associated with the inner

membrane (IM) were missing. A closer investigation of the individual particles revealed that

there was significant variance in the distance between the OM and IM in individual particles,

and that many particles were completely lacking clear densities associated with the IM. It was

therefore decided to create two different sub-tomogram averages with two different masks on

the OM and IM, respectively (37). Those two averages were then juxtaposed together to obtain

a single average with a resolution of 2.4-4.5 nm (figure 7).

The structure of this composite average showed clear similarity with the T4BSS found in

Legionella pneumophila (see figure 8). In the structure there was identified an OM complex and

a periplasmic complex, with a stem-like structure connecting them (figure 7). The OM complex

showed a maximum diameter of ~40nm and had a 13-fold symmetry. A secretion chamber like

that seen in the *L. pneumophila* T4BSS was also observed. The structural similarities that can be

visualized between the *C. burnetii* T4SS and the *L. pneumophila* T4SS are helpful with

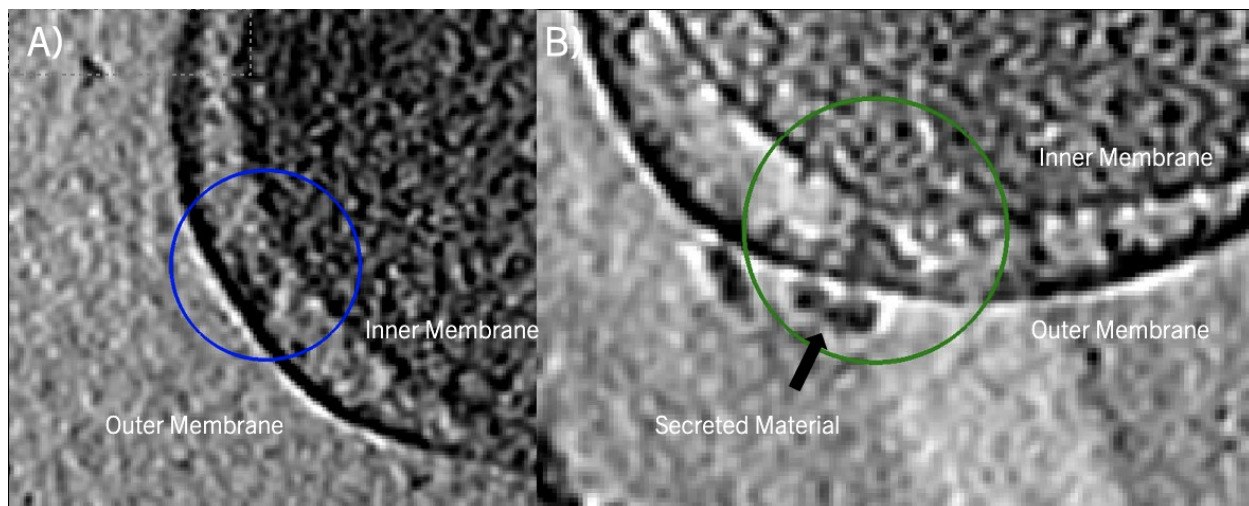confirming proposed ideas about the structure of the *C. burnetii* T4SS.

Fig 6. Secreting and Non-secreting T4BSS Particles in *C. burnetii*

(A) An example of a non-secreting T4SS particle I picked from the *C. burnetii* dataset. Inner/outer membranes labeled for reference. (B) An example of a secreting T4SS particle I picked from the *C. burnetii* dataset. Inner/outer membranes are again labeled. In both cases IM and OM associated densities can be seen, as well as the secretion chamber described above.
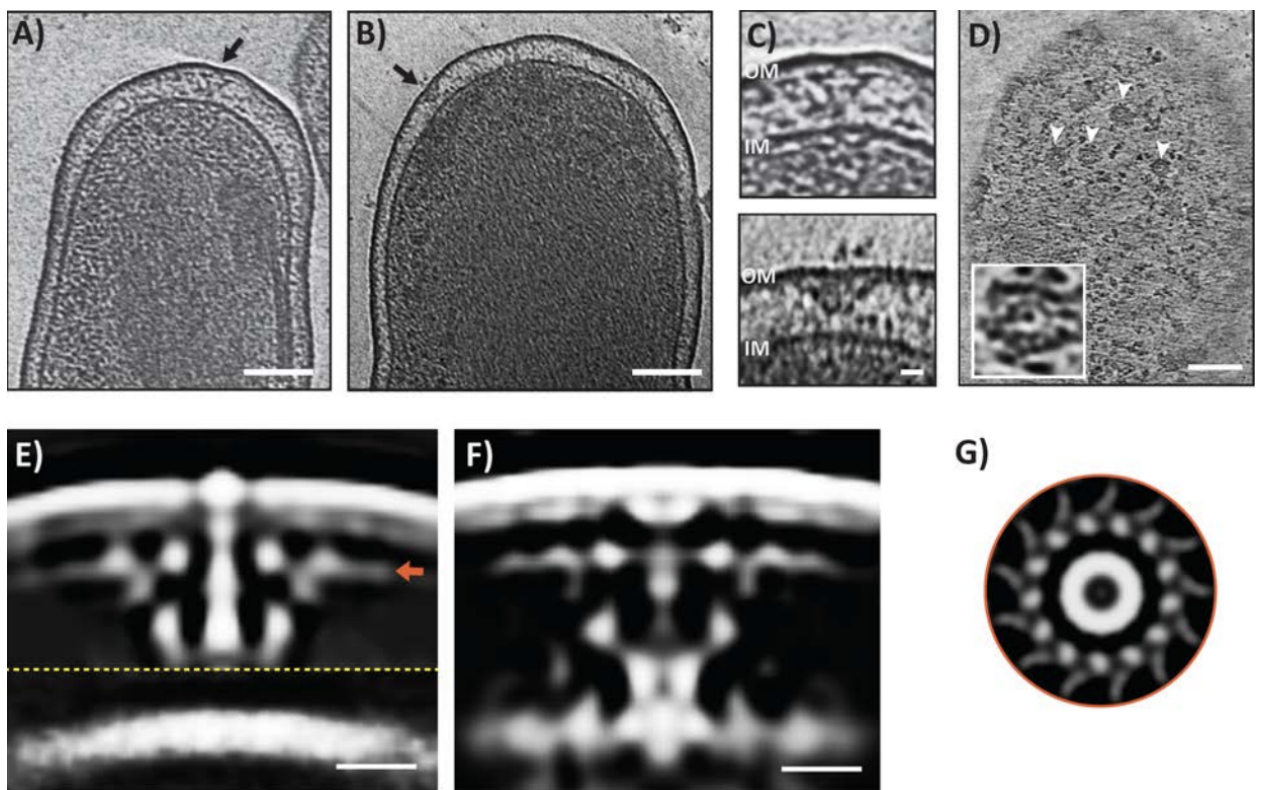

Fig 7. Examples of T4BSS Particles in *C. burnetii*

(A, B) Slices through electron tomograms of *C. burnetii* cells showing the T4BSS complexes *in situ* (black arrows). Scale bar is 100 nm. (C) Enlarged images of the T4BSS complexes shown in images A (top panel) and B (bottom panel). Scale bar is 10 nm. (D) An image of a slice through a partially lysed cell. The circular top perspective T4BSS

structures can clearly be seen. Scale bar is 100 nm. (E, F) Slices through the sub-

tomogram averages of *C. burnetii* at pH 7.2 (left) and pH 4.75 (right). Dashed yellow line

indicates a composite of two averages obtained with different masks (see materials and

methods) concatenated together. Scale bar 10 nm. (G) A cross section through the T4SS

OM complex at position indicated (E, orange arrow) showing 13-fold symmetry (figure
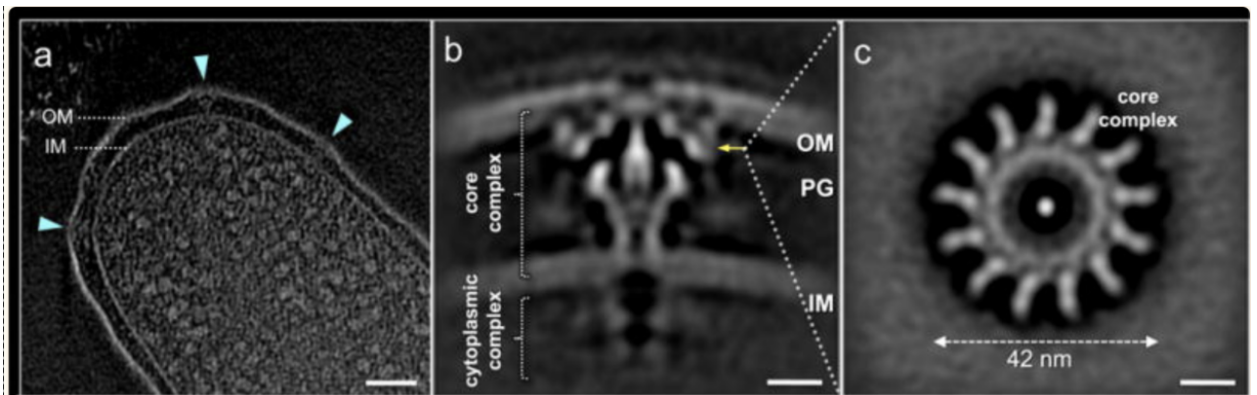
reproduced from (37)).

Fig 7. Examples of T4BSS Particles in *L. pneumophila*

(A) A tomographic slice from a representative *L. pneumophila* cell showing multiple T4SS

embedded in the cell envelope. Note the similarity to the shape of *C. burnetii* T4SS

shown above. Scale var, 100nm. (B) A central section through the longitudinal plane of a

global average structure *in situ* showing the components of the T4BSS in the context of

the outer membrane (OM), the peptidoglycan (PG), and the inner membrane (IM). Scale

bar, 10nm. (C) Cross-section at the position indicated (B, yellow arrow) showing the 13-

fold symmetry. Scale bar 10nm (figure reproduced from (38)).

4. Conclusion

With these projects I was able to use Cryo-ET to observe the T9SS in *P. gingivalis* and the T4SS in *C. burnetii*. I obtained tomograms of these secretion systems and was able to observe their structures. In the T9SS I was able to visualize proteins that have been found using other methods by other researchers. In the T4SS I was able to see and confirm the proposed structural similarity between the *C. burnetii* T4BSS and the *L. pneumophila* T4BSS. These observations coincided with and helped to affirm what has been seen by other researchers about the structural makeup of these secretion systems.

Cryo-ET has proven to be an invaluable tool in the high-resolution structural analysis of bacterial structures. As the available Cryo-ET technologies and experimental techniques have improved, so has our ability to investigate and learn about those structures. Current improvements are centered around issues such as improving data collection time, improving the image detectors, and reducing specimen movement. Advancements in these areas would make it easier to collect large datasets in shorter amounts of time, as well as improve the ever-problematic signal-to-noise ratio of images (34, 35). These improvements will make Cryo-ET an even more valuable tool in bacterial research.

References

1. Murphy G, Jensen G. Electron Cryotomography. BioTechniques. 2018 May;43(4). https://doi.org/10.2144/000112568

2. Oikonomou CM, Swulius MT, Briegel A, Beeby M, YaoQ, Chang YW, Jensen GJ. Chapter 4 - Electron cryotomography. Methods in Microbiology, Academic Press. 2016;43:115-139. https://doi.org/10.1016/bs.mim.2016.10.001.

3. Baumeister W, Grimm R, Walz J. Electron tomography of molecules and cells. Trends in Cell Biology. 1999 Feb;9(2):81-85. https://doi.org/10.1016/S0962-8924(98)01423-8

4. Komeili A, Li Z, Newman DK, Jensen GJ. Magnetosomes are cell membrane invaginations organized by the actin-like protein MamK. Science. 2006 Jan 13;311(5758):242-5. doi:10.1126/science.1123231.https://www.embopress.org/doi/full/10.1038/sj.emboj.7601895

5. Ortega DR, Kjaer A, Briegel A. The chemosensory systems of Vibrio cholerae. Mol Microbiol. 2020 Sep;114(3):367-376. doi: 10.1111/mmi.14520.

6. Beeby M, Cho M, Stubbe J, Jensen G. Growth and Localization of Polyhydroxybutyrate Granules in Ralstonia eutropha. Journal of Bacteriology. 2012; 194(5):1092. DOI: 10.1128/JB.06125-11.

7. Ting CS, Hsieh C, Sundararaman S, Mannella C, Marko M. Electron Cryotomography reveals the comparative three-dimensional architecture of

Prochlorococcus, a globally important marine cyanobacterium. Journal of Bacteriology. 2007 Jun;189(12):4485-4493. DOI: 10.1128/jb.01948-06.

8. Nord. Q Fever, Rare Disease Database. Accessed 2022 Nov 19. https://rarediseases.org/rare-diseases/q-fever/

9. Amano K, Williams JC, McCaul TF, Peacock MG. Biochemical and immunological properties of Coxiella burnetii cell wall and peptidoglycan-protein complex fractions. J Bacteriol. 1984 Dec;160(3):982-8. doi: 10.1128/jb.160.3.982-988.1984.

10. Tang G, Peng L, Baldwin PR, et al. EMAN2: an extensible image processing suite for electron microscopy. Journal of Structural Biology. 2007 Jan;157(1):38-46. DOI: 10.1016/j.jsb.2006.05.009.

11. Ghosal D, Chang YW, Jeong KC, Vogel JP, Jensen GJ. In situ structure of the Legionella Dot/Icm type IV secretion system by electron cryotomography. EMBO Rep. 2017 May 1;18(5):726–32.

12. Graham JG, MacDonald LJ, Hussain SK, Sharma UM, Kurten RC, Voth DE. Virulent Coxiella burnetii pathotypes productively infect primary human alveolar macrophages: Coxiella infection of alveolar macrophages. Cell Microbiol. 2013 Jun;15(6):1012–25

13. Graham JG, MacDonald LJ, Hussain SK, Sharma UM, Kurten RC, Voth DE. Virulent Coxiella burnetii pathotypes productively infect primary human alveolar macrophages: Coxiella infection of alveolar macrophages. Cell Microbiol. 2013 Jun;15(6):1012–25.

14. Coleman SA, Fischer ER, Howe D, Mead DJ, Heinzen RA. Temporal Analysis of Coxiella burnetii Morphological Differentiation. J Bacteriol. 2004 Nov;186(21):7344–52.

15. Hackstadt T, Messer R, Cieplak W, Peacock MG. Evidence for proteolytic cleavage of the 120- kilodalton outer membrane protein of rickettsiae: identification of an avirulent mutant deficient in processing. Infect Immun. 1992 Jan;60(1):159–65.

16. Omsland A, Cockrell DC, Howe D, Fischer ER, Virtaneva K, Sturdevant DE, et al. Host cell-free growth of the Q fever bacterium Coxiella burnetii. Proc Natl Acad Sci. 2009 Mar 17;106(11):4430–4.

17. Omsland A, Beare PA, Hill J, Cockrell DC, Howe D, Hansen B, et al. Isolation from Animal Tissue and Genetic Transformation of Coxiella burnetii Are Facilitated by an Improved Axenic Growth Medium. Appl Environ Microbiol. 2011 Jun;77(11):3720–5.

18. Zheng SQ, Keszthelyi B, Branlund E, Lyle JM, Braunfeld MB, Sedat JW, et al. UCSF tomography: an integrated software suite for real-time electron microscopic tomographic data collection, alignment, and reconstruction. J Struct Biol. 2007 Jan;157(1):138–47.

19. Liu YT, Zhang H, Wang H, Tao CL, Bi GQ, Zhou ZH. Isotropic Reconstruction of Electron Tomograms with Deep Learning [Internet]. Cell Biology; 2021 Jul [cited 2022 Aug 1]. http://biorxiv.org/lookup/doi/10.1101/2021.07.17.452128

20. Gorasia DG, Chreifi G, Seers CA, Butler CA, Heath JE, Glew MD, McBride MJ, Subramanian P, Kjaer A, Jenson GJ, Veith PD, Reynolds Ed. *In situ* structure and

organisation of the type IX secretion system. bioRxiv – Microbiology. 2020
May;094771; https://doi.org/10.1101/2020.05.13.094772

21. Gorasia DG, Veith PD, Reynolds EC. The Type IX Secretion System: Advances in
Structure, Function and Organisation. Microorganisms. 2020 Aug 1;8(8):1173.
doi: 10.3390/microorganisms8081173. PMID: 32752268; PMCID: PMC7463736.

22. Mysak J, Podzimek S, Sommerova P, Lyuya-Mi Y, Bartova J, Janatova T,
Prochazkova J, Duskova J. Porphyromonas gingivalis: major periodontopathic
pathogen overview. J Immunol Res. 2014;2014:476068. doi:
10.1155/2014/476068.

23. How KY, Song KP, Chan KG. Porphyromonas gingivalis: An Overview of
Periodontopathic Pathogen below the Gum Line. Front Microbiol. 2016 Feb
9;7:53. doi: 10.3389/fmicb.2016.00053.

24. Gorasia DG, Veith PD, Hanssen EG, Glew MD, Sato K, Yukitake H, Nakayama K,
Reynolds EC. Structural Insights into the PorK and PorN Components of the
Porphyromonas gingivalis Type IX Secretion System. PLoS Pathog. 2016 Aug
10;12(8):e1005820. doi: 10.1371/journal.ppat.1005820. PMID: 27509186;
PMCID: PMC4980022.

25. Glew MD, Veith PD, Chen D, Gorasia DG, Peng B, Reynolds EC. PorV is an Outer
Membrane Shuttle Protein for the Type IX Secretion System. Sci Rep. 2017 Aug
18;7(1):8790. doi: 10.1038/s41598-017-09412-w.

26. Pickar-Oliver A, Gersbach CA. The next generation of CRISPR-Cas technologies and applications. Nat Rev Mol Cell Biol. 2019 Aug;20(8):490-507. doi: 10.1038/s41580-019-0131-5.

27. Depluverez S, Devos S, Devreese B. The Role of Bacterial Secretion Systems in the Virulence of Gram-Negative Airway Pathogens Associated with Cystic Fibrosis. Front Microbiol. 2016 Aug 30;7:1336. doi: 10.3389/fmicb.2016.01336.

28. Cruz-Morales P, Yin K, Landera A, Cort JR, Young RP, Kyle JE, Bertrand R, Iavarone AT, Acharya S, Cowan A, Chen Y, Gin JW, Scown CD, Petzold CJ, Araujo-Barcelos C, Sundstrom E, George A, Liu Y, Klass S, Nava AA, Keasling JD. Biosynthesis of polycyclopropanated high energy biofuels, Joule. 2022;6(7):1590-1605. https://doi.org/10.1016/j.joule.2022.05.011.

29. Akpe San Roman S, Facey PD, Fernandez-Martinez L, Rodriguez C, Vallin C, Del Sol R, Dyson P. A heterodimer of EsxA and EsxB is involved in sporulation and is secreted by a type VII secretion system in Streptomyces coelicolor. Microbiology (Reading). 2010 Jun;156(Pt 6):1719-1729. doi: 10.1099/mic.0.037069-0. https://www.sciencedirect.com/science/article/pii/S1388248121000874#t0010

30. Obileke K, Onyeaka H, Meyer EL, Nwokolo N. Microbial fuel cells, a renewable energy technology for bio-electricity generation: A mini-review, Electrochemistry Communications. 2021;125:107003. https://doi.org/10.1016/j.elecom.2021.107003.

31. Sedighi M, Zahedi Bialvaei A, Hamblin MR, Ohadi E, Asadi A, Halajzadeh M, Lohrasbi V, Mohammadzadeh N, Amiriani T, Krutova M, Amini A, Kouhsari E.

Therapeutic bacteria to combat cancer; current advances, challenges, and opportunities. Cancer Med. 2019 Jun;8(6):3167-3181. doi: 10.1002/cam4.2148.

32. Vargas G, Cypriano J, Correa T, Leão P, Bazylinski DA, Abreu F. Applications of Magnetotactic Bacteria, Magnetosomes and Magnetosome Crystals in Biotechnology and Nanotechnology: Mini-Review. Molecules. 2018 Sep 24;23(10):2438. doi: 10.3390/molecules23102438.

33. Namba K, Makino F. Recent progress and future perspective of electron cryomicroscopy for structural life sciences. Microscopy (Oxf). 2022 Feb 18;71(Supplement_1):i3-i14. doi: 10.1093/jmicro/dfab049.

34. Vinothkumar KR, Henderson R. Single particle electron cryomicroscopy: trends, issues and future perspective. Q Rev Biophys. 2016 Jan;49:e13. doi: 10.1017/S0033583516000068.

35. Carey KL, Newton HJ, Lührmann A, Roy CR. The Coxiella burnetii Dot/Icm system delivers a unique repertoire of type IV effectors into host cells and is required for intracellular replication. PLoS Pathog. 2011 May;7(5):e1002056. doi: 10.1371/journal.ppat.1002056.

36. Gorasia D, Chreifi G, Seers C, Butler C, Heath J, Glew M, McBride M, Subramanian P, Kjær A, Jensen G, Veith P, Reynolds E. (2020). In situ structure and organisation of the type IX secretion system. bioRxiv. 2020 May;13 doi: 10.1101/2020.05.13.094771.

37. Kaplan M, Shepherd D, Vankadari N, Kim K, Larson C, Dutka P, Beare P, Krzymowski E, Heinzen R, Jensen G, Ghosal D. Structural remodeling of Coxiella

burnetii during its biphasic developmental cycle revealed by cryo-electron
tomography. 2022 August;23 doi: 10.1101/2022.08.23.505044.

38. Chetrit D, Hu B, Christie PJ, Roy CR, Liu J. A unique cytoplasmic ATPase complex
defines the Legionella pneumophila type IV secretion channel. Nat Microbiol.
2018 Jun;3(6):678-686. doi: 10.1038/s41564-018-0165-z. Epub 2018 May 21.
PMID: 29784975; PMCID: PMC5970066.

39. Jonker C. Subtomogram averaging in the cryo-ET workflow. Delmic. 2020
October 2.